第 49 卷 第 24 期/2022 年 12 月/中国激光 研究论文

中国激光

可见光盲 SiC 紫外雪崩光电二极管

杨成东，苏琳琳*，夏开鹏，马文烨

无锡学院电子信息工程学院，江苏 无锡 214105

摘要 SiC 雪崩光电二极管(APD)是用于探测微弱紫外光的优选器件。通过研究器件在高压下的光响应行为，发现随着偏压的增加，器件响应峰值和截止波长始终稳定在 280 nm 和 380 nm 处，表明 SiC APD 在雪崩击穿状态下仍具有可见光盲特性。这说明 SiC APD 在进行微弱紫外光探测时，凭借材料本身性质便可屏蔽可见及红外光的影响，有利于降低器件复杂度和成本。另外，为了增大器件的感光面积，将 SiC APD 直径增大到 500 μm，器件在 95% 击穿电压下，暗电流仅为 2×10^{-10} A，当暗计数为 1 Hz/μm^2 时，器件单光子探测效率为 0.7%，实现了 SiC APD 尺寸上的突破。

关键词 激光器；SiC；雪崩光电二极管；可见光盲；大面积

中图分类号 O47 **文献标志码** A **DOI**：10.3788/CJL202249.2401003

1 引 言

微弱紫外光探测在火灾预警、电晕检测、国防预警和深空检测等领域中有着重要的应用前景[1-5]。雪崩光电二极管(APD)具有高量子效率、高增益和便于集成等优势，成为构建微弱紫外光探测器的首选器件。在材料方面，与 Si 相比，以 GaN 和 SiC 为代表的宽禁带半导体材料能够有效屏蔽可见光和红外光的影响，在紫外探测领域表现出明显优势。其中，GaN 材料的缺陷密度比较大，这导致 GaN APD 的暗电流难以压制[6-7]。此外，GaN APD 在高压下的光响应行为会发生明显红移，相关的研究表明：在 0 V 的工作电压下，GaN APD 的峰值光响应位于 364 nm 处，截止波长为 380 nm，而在 90% 击穿电压时，峰值光响应红移到 370 nm 处，截止波长也拓展到了 440 nm[8]。因此，GaN APD 在进行雪崩探测时将不再具有可见光盲特性。相比较而言，SiC 凭借优异的材料外延技术，能够构建暗电流远低于 GaN 的 APD 器件，该器件是很有应用前景的一种微弱紫外光探测器件[9]。但目前关于 SiC APD 的高压光响应特性研究还鲜有报道，这是关系器件背景噪声的一个关键问题，因此本文将对器件高压下的光响应行为进行研究讨论。

另一方面，由于 APD 工作在雪崩击穿条件下，器件暗电流对材料的缺陷密度十分敏感，即便是低材料缺陷密度的 SiC APD，器件直径也需要控制在 300 μm 以下[10-13]。但是，在进行微弱紫外光探测时，又需要器件具有大的感光面积以提高探测灵敏度。尽管有研究报道了直径为 800 μm 的 SiC APD，但并未给出器件的单光子探测效率这一关键参数，这很可能与材料高缺陷密度引起的高的暗计数有关[14]。本文成功制备了直径为 500 μm 的低暗电流 SiC APD，并且器件仍具有单光子探测性能。

2 器件制备

器件制备在 n 型 4H-SiC 衬底上，如图 1 所示，器件外延结构由下而上分别为一层厚度为 10 μm 的 p 型过渡层(受主掺杂浓度 $N_A=3\times10^{18}$ cm^{-3})，一层厚度为 0.78 μm 的 n−雪崩倍增层(施主掺杂浓度 $N_D=1\times10^{15}$ cm^{-3})，一层厚度为 0.2 μm 的 n 型过渡层($N_D=1\times10^{18}$ cm^{-3})和一层厚度为 0.15 μm 的 n+ 接触层($N_D=1\times10^{19}$ cm^{-3})，器件直径为 150、300、500 μm。为了抑制边缘电场，将器件设计为小角度半台面结构，采用光刻胶回流技术获得倾斜角度为 5°的小倾角台面，并且利用感应耦合等离子体刻蚀系统对外延片进行刻蚀，刻蚀深度为 0.5 μm[9]。为了减少器

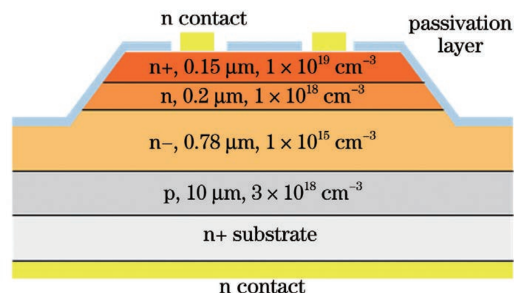

图 1 SiC APD 的剖面结构

Fig. 1 Profile structure of SiC APD

收稿日期：2022-08-01；**修回日期**：2022-09-16；**录用日期**：2022-09-22

基金项目：国家自然科学基金(62106111)、无锡学院引进人才科研启动项目(2021r011，2021r012)

通信作者：*sulinlin@cwxu.edu.cn

件表面漏电，采用 SiO_2 层对外延片表面进行钝化处理，钝化层依次包括牺牲氧化层、热氧化和等离子体增强化学气相沉积（PECVD）生长的厚度为 1 μm 的 SiO_2[15]。最后，利用电子束蒸发系统蒸镀电极，电极金属层依次为 Ni、Ti、Al、Au（厚度分别为 35、50、100、100 nm），随后利用快速热退火系统，将外延片在 850 ℃氮气氛围下退火 3 min 以获得欧姆接触电极。

3 分析与讨论

图 2 描绘了直径为 150 μm 的 SiC APD 在室温下的光电流、暗电流和增益曲线。在雪崩击穿前，器件的暗电流保持在 0.1 pA 量级，对应的暗电流密度为 2.8 nA/cm^2。器件发生雪崩击穿时，光电流和暗电流急剧增加。若把增益达到 1000 时的电压定义为击穿电压，则器件的击穿电压为 260 V。当电压为 264 V 时，器件增益达到 10^6。

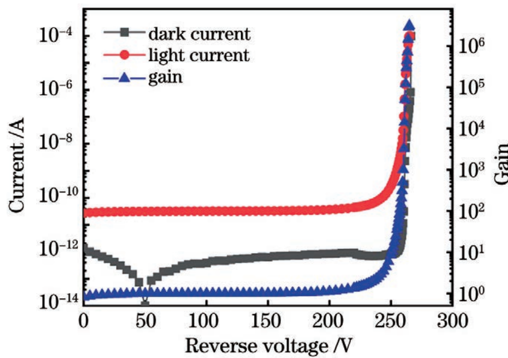

图 2 SiC APD 的电流-电压和增益-电压曲线

Fig. 2 Current-voltage and gain-voltage curves of SiC APD

SiC APD 在进行微弱紫外光探测时，需要工作在雪崩击穿状态下，为了分析器件工作时的可见光盲特性，我们表征了器件在高压下的光响应特性，图 3 所示为 SiC APD 在不同电压下的量子效率曲线。当电压从 0 V 增加到 90%击穿电压（90%U_b）时，SiC APD 的响应峰值始终维持在 280 nm 处，峰值量子效率从 53%增加到 5700%，响应截止波长也保持在 380 nm 处，这与 4H-SiC 材料的禁带宽度相吻合。由此可见，与 GaN APD 相比，SiC APD 在高压下的光响应峰值

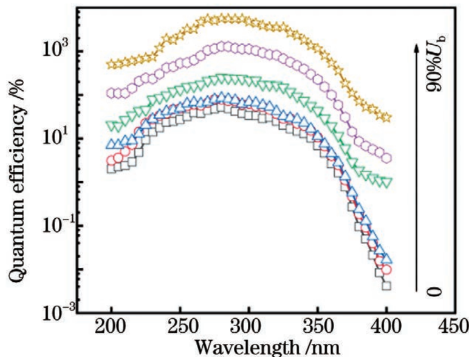

图 3 不同电压下 SiC APD 的量子效率曲线

Fig. 3 Quantum efficiency curves of SiC APD under different voltages

保持不变，不存在光吸收红移行为，光响应范围位于紫外光波段。这证明了 SiC APD 在高电压下仍具有可见光盲特性，凭借材料本身的特性就能有效屏蔽可见光和红外光的影响，大大降低了器件复杂度、体积和成本，是用于微弱紫外光探测的优异器件。

为了提高器件的感光面积，我们同时制备了直径为 300 μm 和 500 μm 的 SiC APD。图 4(a)为不同直径 SiC APD 的暗电流曲线，随着器件尺寸的增加，暗电流增加。SiC APD 的暗电流通常来自表面漏电和体内漏电两部分，通过分析暗电流和器件尺寸的关系可以明确器件漏电来源。图 4(b)为反向偏压为 170 V 时器件暗电流和半径之间的关系曲线，通过拟合发现暗电流与器件的半径成平方关系，这说明器件漏电主要为体内漏电[14]。事实上，SiC APD 的表面漏电一般与材料表面缺陷或表面沾污有关，通过高质量钝化处理能够有效抑制器件表面漏电[15]。造成 SiC APD 体内漏电的可能原因主要有四种：准中性区向耗尽区的反向扩散载流子、耗尽区中的热载流子、带带隧穿和缺陷辅助隧穿。激活能是分析这四个因素的重要依据，当激活能等于材料禁带宽度时，反向扩散载流子是暗电流的主要来源；当激活能为禁带宽度的一半时，耗尽区中的热载流子是暗电流的主要来源；当激活能远小于禁带宽度的一半时，隧穿是暗电流的主要来源[16-18]。

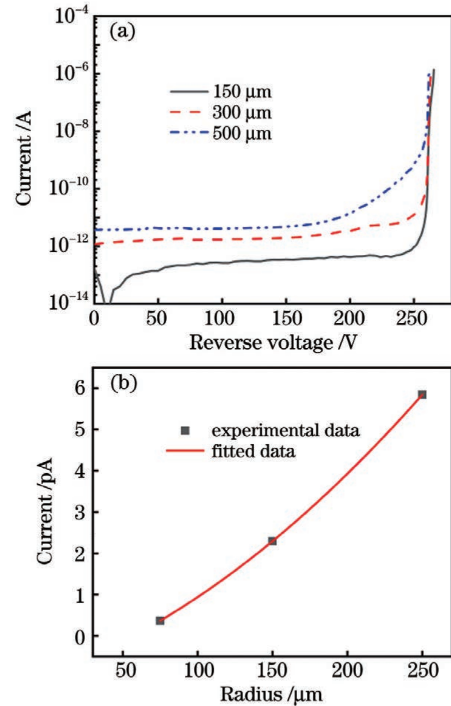

图 4 SiC APD 的暗电流曲线。(a)不同直径 SiC APD 的暗电流曲线；(b)反向偏压为 170 V 时暗电流与半径的关系

Fig. 4 Dark current curves of SiC APD. (a) Dark current curves of SiC APDs with different diameters; (b) dark current as a function of radius at reverse voltage of 170 V

为了进一步分析器件体内漏电的原因，我们测试了 500 μm SiC APD 从室温到 450 K 的暗电流曲线，

如图 5(a)所示，当反向偏压为 200 V 时，器件暗电流从 0.1 nA 增加到 0.7 nA。通过 Arrhenius 方程对反向偏压为 200 V 时的 SiC APD 暗电流进行拟合，如图 5(b)所示(K_B 为玻尔兹曼常数，T 为开尔文温度)，得到激活能为 0.131 eV，远小于禁带宽度的一半(1.63 eV)，这证明了隧穿效应是造成器件暗电流的主要原因。由于 SiC 是一种宽禁带间接带隙半导体，带带隧穿发生的可能性比较低，因此缺陷辅助隧穿是造成 SiC APD 暗电流的主要因素。大量研究工作也表明了 SiC 位错缺陷将会导致 SiC APD 暗电流在高压下显著增加[19]。目前，最优异的 SiC 外延技术能够生长位错密度为 1000～2000 cm^{-2} 的外延片，通过计算发现，对于直径为 500 μm 的器件，最少存在 2～4 个位错，这定会加剧缺陷辅助隧穿，导致暗电流快速增加。因此，材料缺陷密度是制约大尺寸 SiC APD 发展的关键问题。图 6(a) 为 500 μm SiC APD 经熔融 KOH 腐蚀后的光学显微镜形貌图，腐蚀坑扫描电子显微镜图像[图 6(b)]表明缺陷均为六角形穿通型位错，估算的外延片位错密度为 2500～3000 cm^{-2}。图 7 统计了已报道的 SiC APD 在 95% 击穿电压(95%U_b)下的暗电流，对比结果表明，本文制备的 SiC APD 具有更低的暗电流[11,14,20-23]。

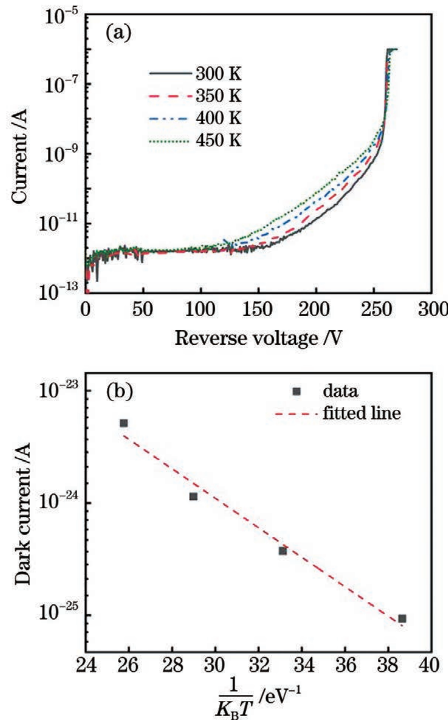

图 5 500 μm SiC APD 的暗电流曲线。(a)不同温度下的暗电流曲线；(b)反向偏压为 200 V 时的暗电流

Fig. 5 Dark current curves of 500 μm SiC APD. (a) Dark current curves at different temperatures; (b) dark current at reverse voltage of 200 V

为了表征器件的单光子探测能力，采用被动淬灭电路表征器件的暗计数和 280 nm 入射光下的光计数，并计算了单光子探测效率[20]。图 8(a)为不同直径

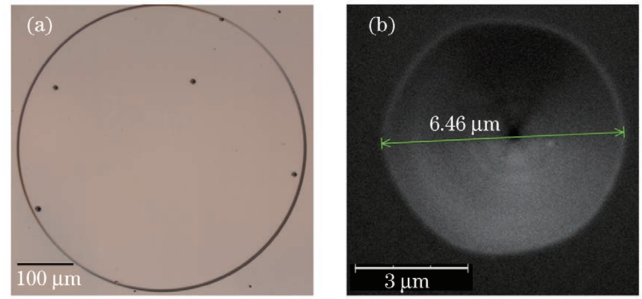

图 6 缺陷图像。(a)光学显微镜图像；(b)扫描电子显微镜图像

Fig. 6 Images of defect. (a) Light microscope image; (b) scanning electron microscope image

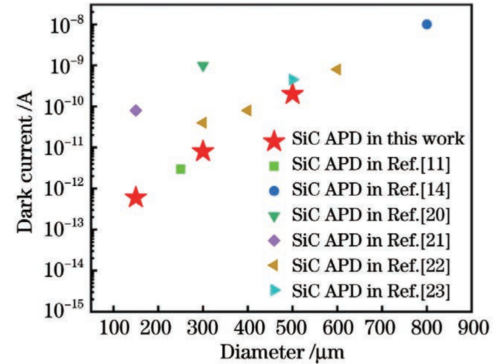

图 7 不同 SiC APD 在 95% 击穿电压下的暗电流比较

Fig. 7 Comparison of dark currents of different SiC APDs at 95%U_b

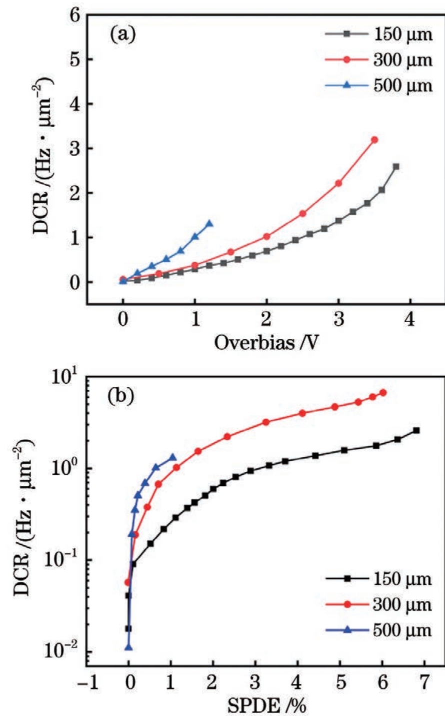

图 8 不同尺寸 SiC APD 的暗计数和单光子探测效率。(a)暗计数-过偏压曲线；(b)暗计数-单光子探测效率曲线

Fig. 8 Dark count rates and single photon detection efficiencies of SiC APDs with different sizes. (a) Dark count rate versus overbias; (b) dark count rate versus single photon detection efficiency

SiC APD 的暗计数曲线，随着器件尺寸的增加，器件的暗计数增加。当 SiC APD 工作在雪崩击穿状态下时，pn 结两端的电压高达 200 V 以上，此时 SiC 能带发生弯曲，载流子发生隧穿效应。大尺寸器件台面内存在更多的缺陷，这会加剧隧穿过程，导致器件暗计数增加。图 8(b)为 SiC APD 的暗计数(DCR)-单光子探测效率(SPDE)曲线，当暗计数为 1 Hz/μm^2 时，150、300、500 μm SiC APD 的单光子探测效率分别为 3.4%、1.2%和 0.7%。目前，已经报道的具有单光子探测能力的 SiC APD 的最大直径为 300 μm，尽管所设计的 500 μm SiC APD 的单光子探测效率还有待提升，但已经实现了器件尺寸上的突破。

4 结　　论

通过研究 SiC APD 在高压下的光响应特性，证明了器件在雪崩击穿状态下仍具有可见光盲特性，比传统的 Si 材料或 GaN 材料更适于微弱紫外光探测。同时，还实现了 SiC APD 感光面积的突破，成功制备了具有单光子探测性能的大面积 SiC APD，器件暗电流优于现有水平，但在今后的工作中仍需要继续优化 SiC 材料质量，以提高器件的单光子探测效率。

参 考 文 献

[1] Wang Y, Qian Y S, Kong X Y. Photon counting based on solar-blind ultraviolet intensified complementary metal-oxide-semiconductor (ICMOS) for corona detection[J]. IEEE Photonics Journal, 2018, 10(6): 1-19.

[2] 赵忆睿，曹念文，贾鹏程，等．紫外多波长激光雷达的臭氧和气溶胶同步观测研究[J]．激光与光电子学进展，2022，59(16)：1601001.
Zhao Y R, Cao N W, Jia P C, et al. Simultaneous observation of ozone and aerosol via ultraviolet multi-wavelength lidar[J]. Laser & Optoelectronics Progress, 2022, 59(16): 1601001.

[3] 袁兆林，胡宇杰，吕季辉，等．ZnO 纳米线阵列/PVK 异质结紫外光探测器特性[J]．光学学报，2022，42(22)：2204001.
Yuan Z L, Hu Y J, Lü J H, et al. Characteristics of ZnO nanowire arrays/PVK heterojunction ultraviolet photodetector[J]. Acta Optica Sinica, 2022, 42(22): 2204001.

[4] 孙立奇，王登魁，房丹，等．CdSe 量子点修饰 ZnO 微米线快速响应的紫外光电探测器[J]．中国激光，2022，49(13)：1303001.
Sun L Q, Wang D K, Fang D, et al. Quantum dots modified ZnO based fast-speed response ultraviolet photodetector[J]. Chinese Journal of Lasers, 2022, 49(13): 1303001.

[5] 王江，罗林保．基于氧化镓日盲紫外光电探测器的研究进展[J]．中国激光，2021，48(11)：1100001.
Wang J, Luo L B. Advances in Ga_2O_3-based solar-blind ultraviolet photodetectors[J]. Chinese Journal of Lasers, 2021, 48(11): 1100001.

[6] Pau J L, McClintock R, Minder K, et al. Geiger-mode operation of back-illuminated GaN avalanche photodiodes[J]. Applied Physics Letters, 2007, 91(4): 041104.

[7] Cicek E, Vashaei Z, McClintock R, et al. Geiger-mode operation of ultraviolet avalanche photodiodes grown on sapphire and free-standing GaN substrates[J]. Applied Physics Letters, 2010, 96(26): 261107.

[8] Shen S C, Zhang Y, Yoo D W, et al. Performance of deep ultraviolet GaN avalanche photodiodes grown by MOCVD[J]. IEEE Photonics Technology Letters, 2007, 19(21): 1744-1746.

[9] Su L L, Zhou D, Lu H, et al. Recent progress of SiC UV single photon counting avalanche photodiodes[J]. Journal of Semiconductors, 2019, 40(12): 65-75.

[10] Vert A, Soloviev S, Sandvik P. SiC avalanche photodiodes and photomultipliers for ultraviolet and solar-blind light detection[J]. Physica Status Solidi (a), 2009, 206(10): 2468-2477.

[11] Bai X G, Liu H D, McIntosh D C, et al. High-detectivity and high-single-photon-detection-efficiency 4H-SiC avalanche photodiodes[J]. IEEE Journal of Quantum Electronics, 2009, 45(3): 300-303.

[12] Zhou D, Liu F, Lu H, et al. High-temperature single photon detection performance of 4H-SiC avalanche photodiodes[J]. IEEE Photonics Technology Letters, 2014, 26(11): 1136-1138.

[13] Li L H, Zhou D, Lu H, et al. 4H-SiC avalanche photodiode linear array operating in Geiger mode[J]. IEEE Photonics Journal, 2017, 9(5): 6804207.

[14] Zhou X Y, Tan X, Wang Y G, et al. High-performance 4H-SiC p-i-n ultraviolet avalanche photodiodes with large active area[J]. Chinese Optics Letters, 2019, 17(9): 090401.

[15] Guo X Y, Beck A L, Li X W, et al. Study of reverse dark current in 4H-SiC avalanche photodiodes[J]. IEEE Journal of Quantum Electronics, 2005, 41(4): 562-567.

[16] Maimon S, Wicks G W. nBn detector, an infrared detector with reduced dark current and higher operating temperature[J]. Applied Physics Letters, 2006, 89(15): 151109.

[17] Ji X L, Liu B Q, Xu Y, et al. Deep-level traps induced dark currents in extended wavelength $In_xGa_{1-x}As$/InP photodetector[J]. Journal of Applied Physics, 2013, 114(22): 224502.

[18] Yang S, Zhou D, Cai X L, et al. Analysis of dark count mechanisms of 4H-SiC ultraviolet avalanche photodiodes working in Geiger mode[J]. IEEE Transactions on Electron Devices, 2017, 64(11): 4532-4539.

[19] Su L L, Zhou D, Liu Q, et al. Effect of a single threading dislocation on electrical and single photon detection characteristics of 4H-SiC ultraviolet avalanche photodiodes[J]. Chinese Physics Letters, 2020, 37(6): 068502.

[20] Zhou X Y, Tan X, Lü Y J, et al. Single-photon-counting performance of 4H-SiC avalanche photodiodes with a wide-range incident flux[J]. IEEE Photonics Technology Letters, 2020, 32(14): 847-850.

[21] Zhou X Y, Tan X, Lü Y J, et al. 128-pixel arrays of 4H-SiC UV APD with dual-frequency PECVD SiN_x passivation[J]. Optics Express, 2020, 28(20): 29245-29252.

[22] Zhou X Y, Li J, Lu W L, et al. Large-area 4H-SiC avalanche photodiodes with high gain and low dark current for visible-blind ultraviolet detection[J]. Chinese Optics Letters, 2018, 16(6): 060401.

[23] Cha H Y, Soloviev S, Zelakiewicz S, et al. Temperature dependent characteristics of nonreach-through 4H-SiC separate absorption and multiplication APDs for UV detection[J]. IEEE Sensors Journal, 2008, 8(3): 233-237.

SiC Visible Light Blindness UV Avalanche Photodiodes

Yang Chengdong, Su Linlin*, Xia Kaipeng, Ma Wenye
School of Electronic Information Engineering, Wuxi University, Wuxi 214105, *Jiangsu, China*

Abstract

Objective High-sensitivity ultraviolet (UV) detectors are required in many critical applications such as corona discharge, missile plume detection, environmental monitoring, and non-line-of-sight communications. As an attractive candidate for weak UV signal detection, avalanche photodiodes (APDs) operating in Geiger mode exhibit promising performance, including small size, low dark current, and high multiplication gain. Wide-bandgap semiconductor materials, such as GaN and SiC, can effectively shield the influence of visible light and infrared light, showing obvious advantages in the field of UV detection. The defect density of GaN is relatively high, which leads to a generally high dark current in GaN APDs. In addition, the photoresponse behavior of GaN APDs under high pressure undergoes a significant red shift, and the cut-off wavelength is extended to 440 nm, indicating the loss of visible light blindness. In comparison, SiC can construct APDs with a much lower dark current than GaN owing to its excellent material epitaxial technology. However, there is still little research on the high-voltage photoresponse characteristics of SiC APDs, which are a key issue related to the background noise of the device. This work discusses the photoresponse behavior of SiC APD under high voltages. Moreover, owing to material defects, the size of the SiC APD is always below 300 μm, but a device with a large photosensitive area is needed to improve the detection sensitivity. Although some studies have reported SiC APDs with a diameter of 800 μm, the key parameter of the single-photon detection efficiency has not been successfully detected. In this study, low-dark-current SiC APDs with a diameter of 500 μm were successfully fabricated, and the devices exhibited single-photon detection performance. This is clearly a breakthrough in terms of the size of SiC APDs.

Methods SiC APDs were fabricated on n-type 4H-SiC substrates (Fig. 1). The epi-structure from bottom to top consists of a 10 μm p+ layer ($N_A=3\times10^{18}$ cm^{-3}), a 0.78 μm n− multiplication layer ($N_D=1\times10^{15}$ cm^{-3}), a 0.2 μm n layer ($N_D=1\times10^{18}$ cm^{-3}), and a 0.15 μm n+ contact layer ($N_D=1\times10^{19}$ cm^{-3}). To suppress peak electrical field around device edge, the beveled mesa with a slope angle of 5° was obtained via photoresist reflow technique, and the mesa was etched down to the multiplication layer by inductively coupled plasma. The device surface was then passivated by thermal oxidation at 1050 ℃ in oxygen atmosphere followed by a 1 μm SiO_2 layer deposited by plasma enhanced chemical vapor deposition at 350 ℃. The n and p type metal stacks, both based on Ni/Ti/Al/Au (35 nm/50 nm/100 nm/100 nm), were deposited by electron-beam evaporation. The devices were then annealed at 850 ℃ for 3 min in N_2 ambient by rapid thermal annealing.

Results and Discussions To analyze whether the SiC APDs still have visible light blindness in the Geiger mode, the photoresponse characteristics of the SiC APD are measured under high voltages. The results show that the response peak of SiC APD is always maintained at 280 nm when the voltage changes from 0% to 90% breakdown voltage (Fig. 3). It is proved that SiC APDs still exhibit visible-light blindness characteristics under high voltages. Owing to the properties of SiC, SiC APD enables the shielding effect of visible and infrared light, which greatly reduces the complexity, volume, and cost of the device. The activation energy of the 500 μm SiC APD is 0.131 eV (Fig. 5), which indicates that the tunneling effect is the main cause of the dark current. At present, the best SiC epitaxy technology can grow epitaxial wafers with a dislocation density of 1000–2000 cm^{-2}. This implies that there are at least 2–4 dislocations in SiC APD with a diameter of 500 μm, which exacerbates defect-assisted tunneling and leads to a rapid increase in dark current. Therefore, the material defect density is a key problem that restricts the development of large-sized SiC APD. The dark current of the reported SiC APDs at 95% breakdown voltage has been calculated, and the comparison shows that the 500 μm SiC APDs fabricated in this work have a lower dark current (Fig. 7). Most importantly, the 500 μm SiC APDs in this work still have the single-photon detection capability. At a dark count rate of 1 Hz/μm^2, the single photon detection efficiency of the device is 0.7%. The most recently reported largest diameter of SiC APD with single-photon detection capability was 300 μm. Although the single-photon detection efficiency of the 500 μm SiC APD reported in this work needs to be improved, a breakthrough in device size has been achieved.

Conclusions In this work, by studying the photoresponse characteristics of SiC APDs under high voltages, it is proved that SiC APDs still exhibit visible light blindness in the avalanche breakdown state, which is more suitable for weak UV light detection than traditional Si or GaN. In addition, we successfully achieve a breakthrough in the photosensitive area of SiC APD and fabricate a large-sized SiC APD with single-photon detection performance. The dark current of the device is better than the existing level. However, to further improve the single-photon detection efficiency of large-sized SiC APDs, it is necessary to optimize the quality of SiC epitaxial wafers in future work.

Key words lasers; SiC; avalanche photodiode; visible light blindness; large area